Device Thrombogenicty Emulator (DTE) – Design optimization Methodology for Cardiovascular Devices: A Study in Two Bileaflet MHV Designs

Michalis Xenos[1], **Gaurav Girdhar**[1], **Yared Alemu**[1], **Jolyon Jesty**[2], **Marvin Slepian**[3], **Shmuel Einav**[1], and **Danny Bluestein**[1,*]

[1] Department of Biomedical Engineering, Stony Brook University, Stony Brook, NY

[2] Division of Hematology, Department of Medicine, Stony Brook University, Stony Brook, NY

[3] Sarver Heart Center, University of Arizona, Tucson, AZ

Abstract

Patients who receive prosthetic heart valve (PHV) implants require mandatory anticoagulation medication after implantation due to the thrombogenic potential of the valve. Optimization of PHV designs may facilitate reduction of flow-induced thrombogenicity and reduce or eliminate the need for post-implant anticoagulants. We present a methodology entitled Device Thrombogenicty Emulator (DTE) for optimizing the thrombo-resistance performance of PHV by combining numerical and experimental approaches. Two bileaflet mechanical heart valves (MHV) designs – St. Jude Medical (SJM) and ATS were investigated, by studying the effect of distinct flow phases on platelet activation. Transient turbulent and direct numerical simulations (DNS) were conducted, and stress loading histories experienced by the platelets were calculated along flow trajectories. The numerical simulations indicated distinct design dependent differences between the two valves. The stress-loading waveforms extracted from the numerical simulations were programmed into a hemodynamic shearing device (HSD), emulating the flow conditions past the valves in distinct 'hot spot' flow regions that are implicated in MHV thrombogenicity. The resultant platelet activity was measured with a modified prothrombinase assay, and was found to be significantly higher in the SJM valve, mostly during the regurgitation phase. The experimental results were in excellent agreement with the calculated platelet activation potential. This establishes the utility of the DTE methodology for serving as a test bed for evaluating design modifications for achieving better thrombogenic performance for such devices.

Keywords

prosthetic heart valves (PHV); mechanical heart valves (MHV); mechanical circulation support (MCS); computational fluid dynamics; platelet activation; platelet assays; thrombogenic performance

1. Introduction

Over 5.3 million patients suffered from heart failure in 2000, with their number expected to grow by 50% over the next 15 years (Lloyd-Jones et al., 2009). Of those, a significant proportion will become candidates for longer-term mechanical circulatory support (MCS), e.g., ventricular assist devices (VAD), total artificial heart (TAH), and prosthetic heart valves. As such a major unmet need is the ability to dramatically reduce the thrombogenic potential of these devices. Mechanical heart valves (MHV) alone correspond to over 170,000 implants worldwide each year (Yoganathan et al., 2005). While hemodynamic performance of current generation of MHVs are greatly improved over their predecessors (DeWall et al., 2000; Bluestein, 2006), flow-induced thrombogenicity is still their major persistent problem (Butchart et al., 2003). To overcome this problem, patients are administered lifelong anti-thrombotic medication, reducing the risk of thrombogenic complications, however increasing hemorrhagic risk.

Blood clotting involves platelet activation and can be initiated by various mechanical and chemical agonists. The non–physiologic flow conditions in MHV (Shandas et al., 2000) have been implicated in activating platelets in the absence of chemical agonists (Hellums et al., 1987) at an approximate threshold shear stress of 100–300 dyne/cm^2 over a few milliseconds (Hung et al., 1976; Ramstack et al., 1979). The Hellums criterion (Hellums et al., 1987; Hellums, 1994) has established a stress exposure time threshold for hemolysis and platelet activation based on constant shear stress experiments. However, under physiological flow conditions of flow through MHVs, platelets are exposed to varying shear stress levels (Bodnar, 1996; Bluestein et al., 1997) and turbulent stresses (Bluestein et al., 2004), as well as repeated passages through the valve that may precipitate activation (Yeleswarapu et al., 1995; Alemu, Bluestein, 2007). The size of the smallest turbulent eddies (Kolmogorov scales) are in the range of 20–70 microns (Ellis et al., 1996; Liu et al., 2000; Travis et al., 2004) and can result in platelet activation (Liu et al., 2000) and initiate thrombosis (Bluestein et al., 2002; Travis et al., 2002; Leytin et al., 2004). Activated platelets with long residence time in these flow regions may aggregate, leading to free emboli formation (Bluestein et al., 2002).

Numerical simulations of MHV flows showed the effects of transient flow and wake dynamics on platelet activation (King et al., 1997; Krafczyk et al., 1998; Kelly et al., 1999; Grigioni et al., 2005a). Many of these simulations assumed laminar flow or neglected intermittent turbulent flow stresses that may become critical in activating the hemostatic system (Bluestein et al., 1997). Valvular flows are dominated by intermittent turbulence in the transition range which are based on isotropic turbulence assumption rendering most turbulence models limited (Yin et al., 2004). Bluestein et al. performed Unsteady Reynolds–averaged Navier–Stokes (URANS) simulations employing the Wilcox k–ω turbulent model, capable of handling transient turbulence (Bluestein et al., 2000; Bluestein et al., 2002) and further compared the activation potentials of various MHVs (Yin et al., 2004) by studying the dynamics of shed vortices in the valve wake and quantifying the stress histories of platelets along pertinent trajectories. Recently, Large Eddy Simulation (LES) (Ge et al., 2003; Ge et al., 2005) and DNS simulations (Dasi et al., 2007; Ge et al., 2008; Nobili et al., 2008a; de Tullio, 2009) were employed, as well as fluid structure interaction (FSI) approaches (Redaelli et al., 2004; Ge et al., 2008). Our group compared the thrombogenic performance of ATS and SJM MHVs using FSI simulations (Dumont et al., 2007).

Mathematical models have been developed to describe the resulting blood damage, mostly focusing at red blood cell (RBC) damage (hemolysis) as opposed to platelet damage (activation), which is more pertinent for thromboembolic complications characterizing MHV (Bludszuweit, 1995; Yeleswarapu et al., 1995; Grigioni et al., 2005b; Farinas et al.,

2006). Those correlate hemoglobin release due to hemolysis, shear stress and exposure time (Pinotti, Rosa, 1995; Arora et al., 2004). Similar platelet activation models are based on percent release of lactate dehydrogenase (LDH) (Arora et al., 2004). These models satisfy limited experimental observations and may significantly underestimate cell damage (Pinotti, Rosa, 1995; Goubergrits, Affeld, 2004).

Previous studies by our group and others have focused on an overall thrombogenic potential measurement in MCS devices (Bluestein et al., 2004; Yin et al., 2004). A limitation of these studies is the lack of specific information regarding the source of elevated platelet activation. It was recently reported that varying the hinge gap in SJM MHVs (Leo et al., 2006) or constriction diameters (Fallon et al., 2008) significantly impact thrombogenicity. These studies reinforce the concept of high shear stress induced platelet activation in constricted geometries.

In the present study we utilize a novel hemodynamic shearing device (HSD) with the capability of accurately reproducing and exposing platelets to rapidly changing dynamic shear stress loading waveforms extracted from detailed numerical simulations. The MHV design specific accentuated effects of such shear stress patterns on platelets is then measured with a modified prothrombinase assay developed by our group for measuring real time thrombin generation due to platelet activation in devices (Jesty, Bluestein, 1999). We have established that the rate of thrombin formation– a universal thrombogenic marker, is directly coupled to the platelet activation level and aggregation that is induced by the flow past valves and devices (Yin et al., 2004; Yin et al., 2005; Yin et al., 2006; Nobili et al., 2008b) and the cardiovascular and mechanical circulatory support device community has long recognized that device thrombogenicity is initiated by platelet activation.

2. Methods

Numerical Simulations

Two MHV designs were compared: a 22 mm AP ATS and a 22 mm SJM 'Regent' valve. Being the most implanted MHV in the world, the SJM is considered as the gold standard (Butany et al., 2003). While their leaflets design closely match, and their inner diameter and nominal orifice sizes are similar (Table 1), they significantly differ in their hinges design, and in the B-datum and valve-housing gap clearances (Dumont et al., 2007). The ATS open pivot design minimizes cavities and recesses in the pivot area of the hinges that may provide locations for platelet aggregation, departing from the St. Jude 'ear' type hinge mechanism (Dumont et al., 2007) (Figure 1). The modeling geometry of the valves consisted of straight tubes upstream and downstream with corresponding lengths of 5 valve diameters. The valves are depicted in closed position, with details of the hinges, housing, and the leaflets (Figure 1). Recent clinical studies have shown that the ATS valve has lower mortality rates and fewer complications as compared to SJM, although there is not currently enough evidence to compare thromboembolic complications rates in the two valves (Bernet et al., 2007; Sezai et al., 2009).

The current study extends our previous one (Dumont et al., 2007) to turbulent and Direct Numerical Simulations (DNS), utilizing highly resolved computational grids in order to capture the smallest scales of the flow. Simulations were carried out during the deceleration phase up to 350 ms from peak systole, before leaflets closure, with the leaflets fixed at the fully open position (Bluestein et al., 2002; Alemu, Bluestein, 2007), corresponding to the phase of the cardiac cycle in which the elevated turbulent stresses and the shed vortices formed in the valve's wake contribute the most to platelet activation and aggregation (Bluestein et al., 2000). Another set of simulations was conducted during the diastolic regurgitant flow phase, which is implicated in thrombus and thromboemboli formation-

especially through the hinges region, with the valve fully closed and a constant velocity of *u* = 0.05*m/s* (Dumont et al., 2007). Blood was assumed to be two-phase Newtonian fluid consisting of fluid carrier phase and neutrally buoyant solid particles representing platelets, as previously described (Bluestein et al., 2002). The stress loading history along flow trajectories experienced by the platelets seeded into the flow field was computed by a summation of the combined effect of the total stress acting on the platelets (a scalar representation of the various components of the stress tensor) and exposure time – as previously described (Alemu, Bluestein, 2007), following the well established shear induced platelet activation (SIPA) concept (Hellums, 1994).

URANS simulations were conducted using the Wilcox *k-ω* turbulence model (Wilcox, 1994; Dhinsa et al., 2005) previously validated by our group experimentally (Bluestein et al., 2000) and applied by us in numerous MHV flow simulations studies (Bluestein et al., 2000; Bluestein et al., 2002; Bluestein et al., 2004; Yin et al., 2004; Alemu, Bluestein, 2007). We have employed a progressive density highly resolved numerical meshes approach (Alemu, Bluestein, 2007) (9×10^6 and 10×10^6 finite volumes for the SJM and the ATS valves, correspondingly) that enabled to accurately capture various hydrodynamic effects in the small confines of MHV complex geometries. Table 1 summarizes valve specifications, diameters and gap clearance for the two designs. The mesh was further refined for the DNS, resulting in over 17×10^6 finite volumes mesh – within the range of previously reported Kolmogorov scales in MHV flows (20–70 μm) (Ellis et al., 1996; Liu et al., 2000; Travis et al., 2004; Ge et al., 2008). A Typical mesh is shown in Figure 2 in two orthogonal sectional planes. Insets in the figure reveal the boundary layers close to the walls. Grid independence was established and results were compared to experimental measurements (see Appendix).

Taking into account the huge number of platelets flowing along multiple trajectories in a complex MHV flow field, an efficient technique is needed to collapse this information into a quantity that could be used for comparing the thrombogenic potential of different valve designs. We introduce herein a new quantitative measure based on computing the Probability Density Function (PDF) of the stress accumulation values of all the trajectories. The PDF is used as a surrogate for the overall thrombogenic potential of each valve, e.g., the MHV thrombogenic 'footprint'. For comparing PDFs of different platelet populations in the various simulations (varying from 15,000 to 50,000), while guaranteeing that the percentage activation is independent of number of seeded particles and spatiotemporal variations, we have used bootstrapping statistics (Dumont et al., 2007) to interpolate between smaller and larger populations. This approach guarantees that the statistical distributions extracted from the different population sizes are compatible and comparable.

Experimental methodology

Platelet trajectories and their corresponding loading shear stress waveforms were extracted from the numerical simulations during the systolic deceleration and regurgitation phases for both MHVs, to be used in the platelet experiments. As only a fraction of the numerous trajectories could possibly be tested experimentally, we have concentrated on 'hot spot' trajectories that are expected to contribute the most to platelet activation. An in-house code was developed that sorted all the trajectories based on specific locations of interest (i.e., gap between valve and housing, B-datum, hinges etc). The localized particle distribution was identified with a sphere of interest, *SOI*, that captured all particle trajectories passing through it. After choosing these 'hot spot' trajectories, their corresponding loading waveforms were programmed into the Hemodynamic Shearing Device (HSD), described below.

We developed a high-torque hemodynamic shearing device (HSD- Figure 3), which combines features of cone and plate and Couette viscometers, to dynamically expose

platelets to uniform shear stress field of rapidly varying levels (Girdhar, Bluestein, 2008). The electrical components of the HSD comprise of a high-torque servo motor-controller system (Baldor Electric Company, AR) with a programmable interface. The shear stress can be changed instantaneously (3 ms resolution), with peak shear stresses up to 900 dyne/cm^2. The motor is mounted onto a mortiser support attached to the cone (Delta, TN and R & W America, IL). The base supports an aluminum block with water recirculation ports, maintaining a physiologic temperature of 37° C. Precise positioning of the cone height above the base-plate is achieved with a dual-bearing-support and the Couette gap between the cone and the ring is controlled with X–Y positioning micrometers. The platelet sample occupies the Couette and the conical spaces. A sample volume of up to 3.5 ml may be used. Platelet activation was measured by sampling from the suspension inside the device before and after the experiment. The HSD was utilized to expose platelets repeatedly (600 times, 10 min) to each dynamic shear stress loading waveforms $\tau(t)$ obtained from numerical simulations. During each successive cycle, platelets were exposed to variable shear stress for 0.21–0.35s, followed by a constant baseline shear stress of 1 dyne/cm^2 for 0.65–0.89s, to keep the platelets in equivalent circulation conditions while not passing through the device. This shear stress level does not activate the platelets and has been used in our previous studies (Nobili et al., 2008b).

30 ml of citrated whole blood was collected from adult human volunteers ($n = 10$ unique donors) after informed consent, in accordance with Stony Brook University Institutional Review Board guidelines. Purified platelets (2×10^8/ml) were prepared by gel-filtration of platelet-rich-plasma (PRP) with a Sepharose-2B column, as previously described (Jesty, Bluestein, 1999). In order to achieve high peak shear stresses in our study, we used Dextran (MW 200,000–500,000; Sigma-Aldrich) to increase viscosity of the suspension to either 3.5 cp (peak stress up to 350 dyne/cm^2) or 10 cp (peak stress up to 900 dyne/cm^2). Platelet activation measurements were performed in the HSD by exposing platelets (2×10^7/ml) to the loading shear stress waveforms. The activation was measured with a Platelet Activity State (PAS) assay developed by our group (Jesty, Bluestein, 1999), which is based on a modified prothrombinase assay. Since platelets from different donors may exhibit high variability in their response to shear stress exposure, the platelet activation measured for any given experimental run was normalized to a maximum value of platelet activation from the same batch by sonication of the platelet suspension at 10W for 10s (Yin et al., 2004; Yin et al., 2005; Yin et al., 2006).

3. Results

Numerical Simulations

Various flow characteristics of the SJM and ATS valve designs are presented and compared. The flow field through the valves is dominated by a triple jet structure through the major orifice (between the leaflets) and the two minor orifices (between the leaflets and the valve housing). At peak systole ATS valve has higher max. velocity ($u_{ATS} = 1.73$ m/s), compared to the SJM ($u_{SJM} = 1.59$ m/s). During regurgitant flow the SJM has a higher max. velocity of 2.99 m/s at the leaflet-housing gap clearance, while the ATS has max. velocity of 2.70 m/s at the gap between the leaflets (B-datum). The flow field at the center plane for the two valves in 3 time instances during the cardiac cycle is depicted in Figure 4. In general, slightly higher velocities and more disturbed flow patterns were observed in the forward flow phase for the ATS valve. However, this was reversed during regurgitant flow phase, in which the SJM valve had stronger flow disturbances, with jets forming at the leaflet-housing gap.

The secondary flow for both valves consisted of a pair of counter-rotating vortices emanating from the jet flow that is generated in the hinges region (Figure 5, traverse cross-

section, with inset zoom in). In an animation of the simulation (Appendix – Animation 1), the spinning of these counter rotating vortices appear to be more rapid for the ATS valve with their axis of rotation entrained towards the core flow. For the SJM valve larger and slower counter rotating vortices were spinning much closer to the valve housing. The formation of these vortices appears to trap a significant number of platelets. The instantaneous vorticity contours at the plane of symmetry of both MHV designs are presented in the Appendix.

The statistical distribution of the stress accumulations along the multiple trajectories was used as the MHV thrombogenic 'footprint', as described above. Both designs have Log-Normal PDF distributions, with different means and variances. The peaks correspond to the mode(s) of each distribution– defined as the value of stress accumulation that most frequently occurs. The mean value of the SJM PDF during the deceleration phase was 4.77 ± 3.23 dyne×s/cm^2 while that of the ATS valve was 8.14 ± 3.57 dyne×s/cm^2. T-test and parametric and non-parametric ANOVA of the two distributions indicate that in the range below 20 dyne×s/cm^2 the SJM valve exposed more platelets to lower stress accumulation values (dominant mode close to 2.0 dyne×s/cm^2 as compared to 4.0 dyne×s/cm^2 for the ATS valve ($p < 0.01$), Figure 6). However, at the higher stress accumulation range (SA > 20 dyne×s/cm^2) the ATS valve appeared to expose very few platelets to values higher than 25 dyne×s/cm^2 (only 0.008% of the trajectories between 25–35 dyne×s/cm^2 for ATS and insignificant 0.006% for the higher 35 dyne×s/cm^2 range). For the SJM valve the percentage at these ranges was significantly higher: 1% of the platelet population was exposed to 25–35 dyne×s/cm^2, and 0.025% to above 35 dyne×s/cm^2 (Figure 6).

During the forward deceleration phase, differences in valve hinge mechanism design resulted in more particles passing through the hinge regions of the ATS, as compared to the SJM valve, 33% and 4% respectively. The mean value of the SJM was 3.02 ± 0.75 dyne×s/cm^2, and 6.43 ± 2.22 dyne×s/cm^2 for the ATS. Specifically, while passing through the hinge area 85% of the SJM trajectories were exposed to low stress accumulation ranges (0–5 dyne×s/cm^2), as compared to only 50% for the ATS. Only 14.8% of the SJM trajectories exposed platelets to higher stress accumulation range (5–25 dyne×s/cm^2), whereas the ATS hinges exposed the rest 50% of the platelets to this higher range. However, for both valves during forward flow no trajectories that pass through the hinges exceeded a cumulative stress of 25 dyne×s/cm^2.

During the diastolic phase of the cardiac cycle, flow through the closed valve is characterized by much higher shear stress values. The two MHV PDF distributions during regurgitation indicate that the ATS valve exposes platelets to much lower stress accumulation levels as compared to the SJM (Figure 7: mean SJM: 1.85 ± 0.4 dyne×s/cm^2, mean ATS 1.2 ± 0.1 dyne×s/cm^2, $p < 0.01$). The dominant mode for the ATS was slightly lower (Figure 7, inset), with 33% of the trajectories passing through the B-datum for the ATS, as compared to only 4% for the SJM. Localized statistics at the B-datum indicated significantly lower mean for ATS (mean ATS: 1.01 dyne×s/cm^2; mean SJM: 1.5 dyne×s/cm^2).

Platelet activation measurements in the HSD

We have previously measured platelet activation in LVAD mounted with bileaflet and monoleaflet MHVs (Yin et al., 2004; Yin et al., 2005). While those studies provided a measure of overall thrombogenicity of the valves, the goal of the current study was to delineate the region specific valve design/geometry effects on platelet activation in the 'hot-spot' regions. A validation study was initially conducted to test the ability of the HSD to emulate stress loadings of region specific trajectories and distinguish the differences in the platelet activity measured (see Appendix).

High stress trajectories were extracted from the hinge regions during the forward flow (1–5 SJM; 6–10 ATS; Figure 8a,b) with their corresponding stress loading waveforms programmed into the HSD and platelet activity measured (Figure 8c: presented as normalized platelet activation values). One-way ANOVA indicated no statistical difference between the two groups of valve trajectories during the forward flow phase (mean platelet activity: 0.0169 ± 0.0011 (SJM); 0.0178 ± 0.0014 (ATS)).

High shear stress trajectories (D1-D3 SJM; D4-D6 ATS) during the regurgitant flow phase were extracted from the B-datum regions (Figure 9). Platelet activation measurements for these trajectories emulated in the HSD show significant difference between the valves, with the SJM overall activation being more than double than the ATS (mean SJM: 0.0275 ± 0.0012; mean ATS: 0.0104 ± 0.0011, $p < 0.05$). Additional high shear stress trajectories from the gap between leaflets and housing regions (W1–W3 SJM; W4–W6 ATS) indicated that the SJM activation level was more than 4 times higher (mean SJM: 0.0665 ± 0.0038; mean ATS: 0.0153 ± 0.0013, $p < 0.05$)

High shear stress trajectories (H1–H3 SJM; H4–H6 ATS) during regurgitant flow were extracted from the hinges regions (Figure 10). The platelet activation measurements for these HSD emulated trajectories show significant difference between the two valves, with the SJM overall activation approx. 5 times higher (mean SJM: 0.0465 ± 0.0023; mean ATS: 0.0090 ± 0.0007, $p < 0.05$).

4. Discussion

The novel DTE (Device Thrombogenicty Emulator) methodology introduced in this work, integrates two approaches - numerical and experimental. In the first step a probability density function (PDF) provides an overall measure of the valve thrombogenic potential ('thrombogenic footprint'), followed by region-specific flow trajectories that are extracted from 'hot-spot' regions. We have demonstrated that this global 'footprint' facilitates a one-to-one comparison of various valve designs. In the second step 'hot spot' trajectories extracted from the numerical simulations are used to program the hemodynamic shearing device (HSD) with the corresponding loading waveforms– emulating extreme flow conditions, and measuring the resultant platelet activity.

The two bileaflet MHV designs, the SJM and ATS, were chosen for illustrating the sensitivity of the methodology in investigating small thrombogenic differences between MHV designs that share many similarities, and differ mostly in their hinge design. High resolution numerical meshes were employed for capturing the smallest scales and realistic valve geometries. Further global and localized statistical analysis of the trajectories was used to quantify the overall and region specific valve thrombogenic performance. We have specifically investigated whether small design variations can produce observable differences in the flow fields and in the resulting platelet activation.

Both MHVs have distinct advantages and disadvantages at various phases of the cardiac cycle. A complex pattern of counter rotating helical vortices was emanating from the hinges region of both valves. Stronger jets during forward flow exposed platelets to slightly higher stresses for the ATS valve. The PDFs indicated that overall the ATS valve is slightly inferior to the SJM valve during the systolic deceleration phase in the $SA < 20$ dyne$\times$s/cm^2. This may be attributed to the design of the SJM valve that diverts the flow trajectories away from the hinges high shear stress region, owing to its 'ear' step design proximal to the hinges. However, in the higher more dangerous range of stress accumulation ($SA > 20$ dyne$\times$s/cm^2) the ATS performs better than the SJM - as depicted in the inset of Figure 6. The corresponding experimental results based on platelet response to representative trajectories

programmed into the HSD however did not yield a statistical difference between the two MHVs. This may be attributed to the small number of loading waveforms chosen from extracted trajectories, and the small difference in the thrombogenicity between the two valves at the forward flow phase, as predicted from the numerical simulations.

During the regurgitant flow through the closed valve the SJM valve exhibited stronger jets around the perimeter of the leaflet-housing gap annular region and through the hinges, whereas the ATS had slightly stronger jets through the B-datum. The size of these high stress regions however was substantially smaller in the ATS valve. The PDF 'footprints' of the stress accumulation during regurgitation correlated very well with the experimental results, with differences in measured platelet activity of all emulated trajectories statistically significant ($p < 0.05$). With similar thrombogenicity during forward flow but much higher thrombogenicity during regurgitant flow, we can confidently state that the SJM valve would be expected to have higher overall thrombogenicity (in agreement with our previous simulations comparing these two valves (Dumont et al., 2007)). The PDF can therefore be used as a predictive measure for the thrombogenic performance 'footprint' characteristic of the specific valve.

While our highly resolved simulations were not conducted as FSI *per se* (Morbiducci et al., 2009), the transient forward flow phase with the leaflets fixed in the fully open position till just before the leaflets snap into closure, fully captures the dynamics essential to platelet activation (e.g., trapping potentially activated platelets in the shed vortices generated in the leaflets' wake). The contribution of the short rapid closing phase (10–20 ms) is expected to be secondary, would be computationally prohibitive for DNS simulations, and for comparative purposes concentrating on the two phases that contribute the most to platelet activation serves the purpose well.

In order to assess statistical turbulence parameters in direct numerical simulations (DNS), the results should be averaged for several cardiac cycles for achieving converged phase-averaged statistics. Statistically, a normal distribution (e.g., the case of isotropic turbulence with Re > 10,000) would require several averaging cycles (depending on the mesh resolution). In case of anisotropic turbulence in the transition range (such as pulsatile flows) a much higher number of cycles may be required to capture the cycle to cycle variations and converge the phase locked turbulent statistics, although a very fine mesh which is resolved below the smallest Kolmogorov turbulent scales may alleviate this requirement. In future simulations we are planning to simulate dozens of cycles for achieving a smaller confidence interval for the turbulence statistics.

Several approximations were made in the numerical simulations. The stress accumulation model utilized for the PDF statistical distributions followed a linear cumulative shear stress approach. However, cumulative shear stress may follow various power-law formulations (Boreda et al., 1995; Nobili et al., 2008b), in which exposure time is given less weight. The linear cumulative shear stress assumption may mask differences that could be attributed to a power-law dependence on peak shear stress, exposure time and stress loading rate. An inherent experimental limitation is that we cannot possibly test the huge number of platelet trajectories generated by the numerical simulations (approx. 15,000–50,000 for each valve). Instead we measure the platelet activation response to a small number of representative stress trajectories that exhibit the highest shear stress levels– serving as a better basis for comparing the two MHV thrombogenic potentials. A high-throughput system with a multiple-HSD setup to study multiple trajectories simultaneously may offer a partial solution in the future.

While for most cases excellent agreement was established between the numerical and experimental results in this study, the correlation is not a function of cumulative shear stress alone. It is apparent from the experimental results presented here that peak shear stress and stress loading rate may also be important parameters that regulate platelet activation. In concurrent and future studies we plan to address these limitations by formulating a more realistic stress accumulation model based on detailed parametric experimental studies, additionally incorporating the effects of repeated passages through the device while taking into account platelet senescence (Alemu, Bluestein, 2007) and sensitization effects (Sheriff et al., 2010).

Our previous studies (Yin et al., 2004; Yin et al., 2005) provided an overall measure of valves thrombogenicity. Moving further, the new methodology presented here is capable of delineating specific effects of the valve design/geometry on platelet activation, either as a stand-alone prosthetic implant or as components of an MCS device. The next step in the DTE methodology is to use this information in order to optimize the design in the 'hot spot' regions. This can be readily achieved by iteratively changing the design in the virtual numerical domain till optimal reduction in the predicted platelet activity is reached, followed by programming the HSD with the loading waveforms resulting from the optimized design and testing to see whether a reduction in platelet activity was indeed achieved. A prototype of the optimized device can then be fabricated and clinically tested.

In conclusion, we have demonstrated the efficacy of our methodology for estimating the effects of design parameters on device thrombogenicity. We envision that this methodology will be adopted by cardiovascular device manufacturers in order to optimize their devices designs for achieving improved thrombogenic performance. This may reduce or even eliminate the need for anticoagulation that is mandated for most of these devices.

Supplementary Material

Refer to Web version on PubMed Central for supplementary material.

Acknowledgments

References

Alemu Y, Bluestein D. Flow-induced platelet activation and damage accumulation in a mechanical heart valve: numerical studies. Artificial Organs. 2007; 31(9):677–688. [PubMed: 17725695]

Apel J, Neudel F, Reul H. Computational fluid dynamics and experimental validation of a microaxial blood pump. ASAIO Journal. 2001; 47(5):552–558. [PubMed: 11575836]

Arora D, Behr M, Pasquali M. A Tensor-based Measure for Estimating Blood Damage. Artificial Organs. 2004; 28(11):1002–1015. [PubMed: 15504116]

Bernet FH, Baykut D, Grize L, Zerkowski HR. Single-center outcome analysis of 1,161 patients with St. Jude medical and ATS open pivot mechanical heart valves. Journal of Heart Valve Disease. 2007; 16(2):151–158. [PubMed: 17484464]

Bludszuweit C. Model for a general mechanical blood damage prediction. Artificial Organs. 1995; 19(7):583–589. [PubMed: 8572956]

Bluestein D. Towards optimization of the thrombogenic potential of blood recirculating cardiovascular devices using modeling approaches. Expert Review of Medical Devices. 2006; 3(3):267–270. [PubMed: 16681446]

Bluestein D, Li YM, Krukenkamp IB. Free emboli formation in the wake of bi-leaflet mechanical heart valves and the effects of implantation techniques. Journal of Biomechanics. 2002; 35(12):1533–40. [PubMed: 12445606]

Bluestein D, Niu L, Schoephoerster RT, Dewanjee MK. Fluid mechanics of arterial stenosis: relationship to the development of mural thrombus. Annals of Biomedical Engineering. 1997; 25(2): 344–56. [PubMed: 9084839]

Bluestein D, Rambod E, Gharib M. Vortex shedding as a mechanism for free emboli formation in mechanical heart valves. Journal of Biomechanical Engineering. 2000; 122(2):125–134. [PubMed: 10834152]

Bluestein D, Yin W, Affeld K, Jesty J. Flow-induced platelet activation in mechanical heart valves. Journal of Heart Valve Disease. 2004; 13(3):501–508. [PubMed: 15222299]

Bodnar E. The Medtronic Parallel valve and the lessons learned. Journal of Heart Valve Disease. 1996; 5(6):572–573. [PubMed: 8953433]

Boreda R, Fatemi RS, Rittgers SE. Potential for platelet stimulation in critically stenosed carotid and coronary arteries. Journal of Vascular Investigation. 1995; 1:26–37.

Butany J, Ahluwalia MS, Munroe C, Fayet C, Ahn C, Blit P, Kepron C, Cusimano RJ, Leask RL. Mechanical heart valve prostheses: identification and evaluation. Cardiovascular Pathology. 2003; 12(1):1–22. [PubMed: 12598013]

Butchart EG, Ionescu A, Payne N, Giddings J, Grunkemeier GL, Fraser AG. A new scoring system to determine thromboembolic risk after heart valve replacement. Circulation. 2003; 108(Suppl 1):II68–74. [PubMed: 12970211]

Dasi LP, Ge L, Simon HA, Sotiropoulos F, Yoganathan AP. Vorticity dynamics of a bileaflet mechanical heart valve in an axisymmetric aorta. Physics of Fluids. 2007; 19(6):1–17.

de Tullio MD, Cristallo A, Balaras E, Verzicco R. Direct numerical simulation of the pulsatile flow through an aortic bileaflet mechanical heart valve. Journal of Fluid Mechanics. 2009; 622:259–290.

DeWall RA, Qasim N, Carr L. Evolution of mechanical heart valves. Ann Thorac Surg. 2000; 69(5): 1612–1621. [PubMed: 10881865]

Dhinsa K, Bailey C, Pericleous K. Investigation into the performance of turbulence models for fluid flow and heat transfer phenomena in electronic applications. IEEE Transactions on Components and Packaging Technologies. 2005; 28(4):686–699.

Dumont K, Vierendeels J, Kaminsky R, van Nooten G, Verdonck P, Bluestein D. Comparison of the hemodynamic and thrombogenic performance of two bileaflet mechanical heart valves using a CFD/FSI model. Journal of Biomechanical Engineering. 2007; 129(4):558–565. [PubMed: 17655477]

Ellis JT, Healy TM, Fontaine AA, Saxena R, Yoganathan AP. Velocity measurements and flow patterns within the hinge region of a Medtronic Parallel bileaflet mechanical valve with clear housing. Journal of Heart Valve Disease. 1996; 5(6):591–599. [PubMed: 8953436]

Fallon AM, Dasi LP, Marzec UM, Hanson SR, Yoganathan AP. Procoagulant properties of flow fields in stenotic and expansive orifices. Annals of Biomedical Engineering. 2008; 36(1):1–13. [PubMed: 17985244]

Farinas MI, Garon A, Lacasse D, N'dri D. Asymptotically consistent a numerical approximation of hemolysis. Journal of Biomechanical Engineering-Transactions of the ASME. 2006; 128(5):688–696.

Ge L, Dasi LP, Sotiropoulos F, Yoganathan AP. Characterization of hemodynamic forces induced by mechanical heart valves: Reynolds vs. viscous stresses. Annals of Biomedical Engineering. 2008; 36(2):276–297. [PubMed: 18049902]

Ge L, Jones SC, Sotiropoulos F, Healy TM, Yoganathan AP. Numerical simulation of flow in mechanical heart valves: grid resolution and the assumption of flow symmetry. Journal of Biomechanical Engineering. 2003; 125(5):709–718. [PubMed: 14618930]

Ge L, Leo HL, Sotiropoulos F, Yoganathan AP. Flow in a mechanical bileaflet heart valve at laminar and near-peak systole flow rates: CFD simulations and experiments. Journal of Biomechanical Engineering. 2005; 127(5):782–797. [PubMed: 16248308]

Girdhar G, Bluestein D. Biological effects of dynamic shear stress in cardiovascular pathologies and devices. Expert Review of Medical Devices. 2008; 5(2):167–181. [PubMed: 18331179]

Goubergrits L, Affeld K. Numerical estimation of blood damage in artificial organs. Artificial Organs. 2004; 28(5):499–507. [PubMed: 15113346]

Grigioni M, Daniele C, Del Gaudio C, Morbiducci U, Balducci A, D'Avenio G, Barbaro V. Three-dimensional numeric simulation of flow through an aortic bileaflet valve in a realistic model of aortic root. ASAIO Journal. 2005a; 51(3):176–183. [PubMed: 15968945]

Grigioni M, Morbiducci U, D'Avenio G, Di Benedetto G, Del Gaudio C. A novel formulation for blood trauma prediction by a modified power-law mathematical model. Biomechanics and Modeling in Mechanobiology. 2005b; 4(4):249–260. [PubMed: 16283225]

Hellums JD. 1993 Whitaker Lecture: biorheology in thrombosis research. Annals of Biomedical Engineering. 1994; 22(5):445–455. [PubMed: 7825747]

Hellums, JD.; Peterson, DM.; Stathopoulos, NA.; Moake, JL.; Giorgio, TD. Studies on the mechanisms of shear-induced platelet activation. New York: Springer and Verlag; 1987.

Hung TC, Hochmuth RM, Joist JH, Sutera SP. Shear-induced aggregation and lysis of platelets. Transactions of the ASAIO. 1976; 22:285–291.

Jesty J, Bluestein D. Acetylated prothrombin as a substrate in the measurement of the procoagulant activity of platelets: elimination of the feedback activation of platelets by thrombin. Analytical Biochemistry. 1999; 272(1):64–70. [PubMed: 10405294]

Kelly SG, Verdonck PR, Vierendeels JA, Riemslagh K, Dick E, Van Nooten GG. A three-dimensional analysis of flow in the pivot regions of an ATS bileaflet valve. International Journal Artificial Organs. 1999; 22(11):754–763.

King MJ, David T, Fisher J. Three-dimensional study of the effect of two leaflet opening angles on the time-dependent flow through a bileaflet mechanical heart valve. Medical Engineering & Physics. 1997; 19(3):235–241. [PubMed: 9239642]

Krafczyk M, Cerrolaza M, Schulz M, Rank E. Analysis of 3D transient blood flow passing through an artificial aortic valve by Lattice-Boltzmann methods. Journal of Biomechanics. 1998; 31(5):453–462. [PubMed: 9727343]

Leo HL, Simon HA, Dasi LP, Yoganathan AP. Effect of hinge gap width on the microflow structures in 27-mm bileaflet mechanical heart valves. Journal of Heart Valve Disease. 2006; 15(6):800–808. [PubMed: 17152788]

Leytin V, Allen DJ, Mykhaylov S, Mis L, Lyubimov EV, Garvey B, Freedman J. Pathologic high shear stress induces apoptosis events in human platelets. Biochemical & Biophysical Research Communications. 2004; 320(2):303–310. [PubMed: 15219827]

Liu JS, Lu PC, Chu SH. Turbulence characteristics downstream of bileaflet aortic valve prostheses. Journal of Biomechanical Engineering. 2000; 122(2):118–124. [PubMed: 10834151]

Lloyd-Jones D, Adams R, Carnethon M, De Simone G, Ferguson TB, Flegal K, Ford E, Furie K, Go A, Greenlund K, Haase N, Hailpern S, Ho M, Howard V, Kissela B, Kittner S, Lackland D, Lisabeth L, Marelli A, McDermott M, Meigs J, Mozaffarian D, Nichol G, O'Donnell C, Roger V, Rosamond W, Sacco R, Sorlie P, Stafford R, Steinberger J, Thom T, Wasserthiel-Smoller S, Wong N, Wylie-Rosett J, Hong Y. Heart disease and stroke statistics--2009 update: a report from the American Heart Association Statistics Committee and Stroke Statistics Subcommittee. Circulation. 2009; 119(3):e21–181. [PubMed: 19075105]

Morbiducci U, Ponzini R, Nobili M, Massai D, Montevecchi FM, Bluestein D, Redaelli A. Blood damage safety of prosthetic heart valves. Shear-induced platelet activation and local flow dynamics: a fluid-structure interaction approach. Journal of Biomechanics. 2009; 42(12):1952–1960. [PubMed: 19524927]

Morsi SA, Alexander AJ. An Investigation of Particle Trajectories in 2-Phase Flow Systems. Journal of Fluid Mechanics. 1972; 55:193–208.

Nobili M, Morbiducci U, Ponzini R, Del Gaudio C, Balducci A, Grigioni M, Montevecchi FM, Redaelli A. Numerical simulation of the dynamics of a bileaflet prosthetic heart valve using a fluid-structure interaction approach. Journal of Biomechanics. 2008a; 41(11):2539–2550. [PubMed: 18579146]

Nobili M, Sheriff J, Morbiducci U, Redaelli A, Bluestein D. Platelet activation due to hemodynamic shear stresses: damage accumulation model and comparison to in vitro measurements. ASAIO Journal. 2008b; 54(1):64–72. [PubMed: 18204318]

Pinotti M, Rosa ES. Computational Prediction of Hemolysis in a Centrifugal Ventricular Assist Device. Artificial Organs. 1995; 19(3):267–273. [PubMed: 7779017]

Ramstack JM, Zuckerman L, Mockros LF. Shear-induced activation of platelets. Journal of Biomechanics. 1979; 12(2):113–125. [PubMed: 422576]

Redaelli A, Bothorel H, Votta E, Soncini M, Morbiducci U, Del Gaudio C, Balducci A, Grigioni M. 3-D simulation of the St. Jude Medical bileaflet valve opening process: fluid-structure interaction study and experimental validation. Journal of Heart Valve Disease. 2004; 13(5):804–813. [PubMed: 15473484]

Sezai A, Hata M, Niino T, Yoshitake I, Kasamaki Y, Hirayama A, Minami K. Fifteen years of experience with ATS mechanical heart valve prostheses. Journal of Thoracic Cardiovascular Surgery. 2009

Shandas R, Kwon J, Valdes-Cruz L. A method for determining the reference effective flow areas for mechanical heart valve prostheses: in vitro validation studies. Circulation. 2000; 101(16):1953–1959. [PubMed: 10779462]

Sheriff J, Bluestein D, Girdhar G, Jesty J. High-Shear Stress Sensitizes Platelets to Subsequent Low-Shear Conditions. Annals of Biomedical Engineering. 2010; 38(4):1442–1450. [PubMed: 20135353]

Travis BR, Christensen TD, Smerup M, Olsen MS, Hasenkam JM, Nygaard H. An in vivo method for measuring turbulence in mechanical prosthesis leakage jets. Journal of Biomechanical Engineering-Transactions of the ASME. 2004; 126(1):26–35.

Travis BR, Leo HL, Shah PA, Frakes DH, Yoganathan AP. An analysis of turbulent shear stresses in leakage flow through a bileaflet mechanical prostheses. Journal of Biomechanical Engineering. 2002; 124(2):155–165. [PubMed: 12002124]

Wilcox DC. Simulation of transition with a two-equation turbulence model. AIAA Journal. 1994; 32(2):247–255.

Yeleswarapu KK, Antaki JF, Kameneva MV, Rajagopal KR. A mathematical model for shear-induced hemolysis. Artificial Organs. 1995; 19(7):576–582. [PubMed: 8572955]

Yin W, Alemu Y, Affeld K, Jesty J, Bluestein D. Flow-induced platelet activation in bileaflet and monoleaflet mechanical heart valves. Annals of Biomedical Engineering. 2004; 32(8):1058–1066. [PubMed: 15446502]

Yin W, Gallocher S, Pinchuk L, Schoephoerster RT, Jesty J, Bluestein D. Flow Induced Platelet Activation in a St. Jude MHV, a Trileaflet Polymeric Heart Valve and a St. Jude Tissue Valve. Artificial Organs. 2005; 29(10):826–831. [PubMed: 16185345]

Yin W, Krukenkamp IB, Saltman AE, Gaudette G, Suresh K, Bernal O, Jesty J, Bluestein D. The Thrombogenic Performance of a St. Jude Bileaflet MHV in a Sheep Model. ASAIO Journal. 2006; 52(1):28–33. [PubMed: 16436887]

Yoganathan AP, Chandran KB, Sotiropoulos F. Flow in prosthetic heart valves: state-of-the-art and future directions. Annals of Biomedical Engineering. 2005; 33(12):1689–1694. [PubMed: 16389514]

Appendix

The appendix incorporates technical details regarding the DTE methodology such as grid and time independency studies, validation of the velocity profiles with experimental data and details about the computation of the platelet trajectories. Numerical results concerning the instantaneous vorticity and turbulent intensities of the two MHV designs are also included. A validation study of the HSD is also presented.

Models geometry

In this comparative study, the aortic sinuses were excluded from the model. Aortic valve replacement (AVR) requires partially dissecting the aortic root sinuses, so that after MHV implantation only a portion of the sinuses remain (unlike the native aortic valve, MHV do not utilize the sinus vortex as a part of their opening and closing mechanism). Including the aortic root may alter the flow field influencing the stresses distal the valve (Grigioni et al., 2005a). However, the focus of the current study is to investigate comparatively and specifically the influence of small design changes in MHV geometry itself, and to demonstrate the capability of the DTE methodology to identify the least thrombogenic valve design independent of other geometric parameters that are not specific to the valve itself. Both valves were fully open (85°) during peak systole, and fully closed during the regurgitant flow phase (closing angle of 60.2° for SJM, and 62.6° for the ATS) - leaving a corresponding regurgitation gap (Table 1).

Grid and time Independence studies

Grid and time step independence studies were conducted using three different grid sizes of 2, 9 and 17×10^6 cells (Figure 11). Results were compared at two axial locations: **A-** proximal to the valve and **B-** right distal to the valve leaflets (Figure 12). We also compared DNS results with a turbulent simulation using the 9 million finite volumes grid. At cross-section **A** (upstream) all computational grids provided similar results, the difference between the 17 million elements grid and the 9 million elements grid was 0.7% where the difference between the 17 million elements grid and the 2 million elements grid was 1.0%. At cross-section **B** the difference increased slightly, for the first case (17 million elements versus 9 million elements) the difference was 1.3%, for the second case (17 million elements versus 2 million elements) the difference was 4%. All simulations were therefore conducted with the 9 million elements computational grid.

In the current study a formulation which is based on two energy partitions system that is able to account for sudden changes in mean-strain rate — a shortcoming of the various high-Re k-ε -type turbulence models was employed. The turbulent terms are handled using the two additional equations from the Wilcox k–ω model, with the values of the turbulent constants employed given in Table 2. Progressive density mesh was used to resolve boundary layer flow near all solid boundaries as required by the turbulence model. The minimal mesh density in the near wall region was dictated by the need in the k-ω model of the first grid point away from the walls to be $y^+ \leq 1$ (y^+ - non dimensional viscous sub-layer height). The height of Δ - the first grid point from the wall, was computed according to: $\omega = 6v/\beta\Delta^2$ (Wilcox, 1994) and put Δ at a characteristic value of under 100 μm (Alemu, Bluestein, 2007), which was used to establish the minimal mesh density in the near wall region (where v is the kinematic viscosity and β a constant of the k-ω model). This was finely tuned to a value of 70 μm.

Transient simulations were performed with different time steps to identify the best step size. After establishing that the difference in the velocity profiles at the same locations between dt = 0.0005 s and dt = 0.001 s was smaller than 5%, all simulations were performed with a time step of dt = 0.0005 s.

Validation with experimental data

The velocity results obtained from the DNS simulations were compared with experimental data from the literature (Ge et al., 2005) measured using particle image velocimetry (PIV) in a similar SJM MHV design, under a similar flow configuration. Dimensionless velocity

profiles from our simulations at a cross section exactly downstream the tip of the leaflets (**B** location, Figure 12) are in very good agreement with the experimental measurements (at three vertical planes, y = 0, 0.3*R* and 0.6*R*, *R*- valve radius).

Computation of the platelet trajectories

Blood was assumed to be two-phase Newtonian fluid consisting of fluid carrier phase and neutrally buoyant solid particles representing blood platelets (density of the particles assumed similar to blood density). Two-phase formulation which takes into account the particle-fluid interaction was employed. It predicts the trajectories of the discrete phase particles (platelets) by integrating the force balance on the particles in a Lagrangian reference frame, according to equation (1).

$$\frac{d\vec{q}_p}{dt} = F_D\left(\vec{q} - \vec{q}_p\right) + \vec{F}, \text{ momentum for particles} \tag{1}$$

$$\text{where:} F_D = \frac{18\mu}{\rho_p d_p^2} \frac{C_D \text{Re}}{24} \text{ and } \text{Re} = \frac{\rho d_p |\vec{q}_p - \vec{q}|}{\mu}. \tag{2}$$

The first term $F_D(\vec{q} - \vec{q}_p)$ in equation (1) is the drag force acting on the particles due to the relative fluid motion, and $\vec{F}$ is the inertial momentum, with the drag force F_D formulated as a function of the Reynolds number. In the above equations $\vec{q}$ is the fluid velocity vector, $\vec{q}_p$ the platelet velocity vector, μ, ρ are the viscosity and density of the fluid, ρ_p is the density of the platelets with a spherical diameter of $d_p = 3\mu m$. C_D is the drag coefficient of a smoothed spherical particle (Morsi, Alexander, 1972) and Re is the relative Reynolds number defined in equation (2).

Stress accumulation (SA)

Flow results from the simulations were used to calculate the stress loading history experienced by the seeded platelets in the flow field, by computing the combined effect of stress and exposure time following the well established shear induced platelet activation (SIPA) concept. The dynamic combinations of loading and exposure times, and the contribution of the various components of the stress tensor, e.g. laminar and turbulent stress tensors, have been incorporated into a stress accumulation model.

The total stress is reduced to a scalar value according to equation (4), where τ_{ij} are the components of the stress tensor, as previously described (Alemu, Bluestein, 2007). For laminar simulations the stress tensor is extracted from the laminar viscous shear stress (first term in equation (3)), while for turbulent simulations the additional *Reynolds stresses* were calculated using the *Boussinesq* approximation (Alemu, Bluestein, 2007), (second term of equation (3)) according to:

$$\tau_{ij} = \underbrace{\mu\left(\frac{\partial u_i}{\partial x_j} + \frac{\partial u_j}{\partial x_i}\right)}_{\text{laminar}} - \underbrace{v_t(\rho\overline{u_i'u_j'})}_{\text{turbulent}}, \ \tau_{turb\ ij} = -\rho\overline{u_i'u_j'} \approx \mu_t\left(\frac{\partial u_i}{\partial x_j} + \frac{\partial u_j}{\partial x_i}\right) - \frac{2}{3}\left(\rho k + \mu_t\frac{\partial u_k}{\partial x_k}\right)\delta_{ij}, \tag{3}$$

The components of the stress tensor are then rendered into a scalar stress value (Apel et al., 2001), according to:

$$\sigma = \frac{1}{\sqrt{3}} \sqrt{\tau_{11}^2 + \tau_{22}^2 + \tau_{33}^2 - \tau_{11}\tau_{22} - \tau_{11}\tau_{33} - \tau_{22}\tau_{33} + 3\left(\tau_{12}^2 + \tau_{23}^2 + \tau_{13}^2\right)}$$

(4)

The stress accumulation calculation is then performed by a summation of the instantaneous product of this scalar value of the total stress and the exposure time between successive nodal points along the platelet trajectory:

$$SA = \int_{t_0}^{t} \sigma(t)dt \approx \sum_{i=1}^{N} \sigma_i \times \Delta t.$$

(5)

Where σ_i, $i = 1, \ldots, N$ is the nodal scalar value extracted from the total stress tensor as described above and Δt the corresponding time step between the successive nodal points. Localized statistical stress accumulation distributions for the hinge regions were used to compare the two MHV designs during forward and regurgitant flows. For the localized particle statistics a sphere of interest, *SOI*, located at the middle of the hinge and with a radius, *r*, of 2.5mm was used to capture all particle trajectories passing through.

Instantaneous vorticity

Snapshots of the instantaneous vorticity contours, ω_x, at the plane of symmetry, $z = 0$, for both valves are depicted in Figure 13, reveal highly unsteady flow fields for both valves. During the deceleration phase, elongated shear layers that extend farther downstream of the leaflet are noticeable for the SJM valve. The ATS valve has substantially shorter shear layers. The SJM valve exhibits higher levels of vorticity in the leaflet-housing gap region during the regurgitant flow phase. ATS valve reveals a different vorticity pattern, with highest vorticity levels at the B-datum gap and lower at the leaflet-housing gap (Figure 13).

Turbulent intensity of the MHV designs

Turbulent intensity, *Tu*, is the measure of flow disturbance that correlates with the averaged mean and fluctuating velocity components. The inlet turbulent intensity was assumed to be very small ($Tu_{inlet} = 1 \times 10^{-4}$). This is a valid approximation given that most of the turbulence is generated by the valve itself rather than free stream turbulent intensity. Values of *Tu* were extracted from both the SJM and ATS simulation results during peak systole, and at 130ms and 270ms after peak systole. In the SJM valve the *Tu* value is initially 26.9%, dropping to 14.7% around 270ms. At peak systole the ATS valve has 13.3% *Tu*, dropping to 8.9% around 270ms. For both valves, the leading edge, where flow first encounters the valve leaflets and the hinge regions are identified as the locations with the highest *Tu* values.

Validation study of the HSD

A validation study was conducted in the SJM valve to test whether location-specific platelet activity (corresponding to distinct flow regions) measured in the HSD with emulated loading waveforms, could be distinguished based on locations. To that end, two distinct flow regions were compared – 'core' flow with its characteristic low stress accumulation levels, as compared to the flow near the hinges and the walls (non-core flow regions- with its substantially higher levels of shear stresses).

Several of these trajectories that were extracted from the numerical simulations performed in the SJM valve were chosen for the platelet experiments in the HSD (Figure 14a), spatially

organized according to 'core' flow - close to the center of the valve (1 and 2), and 'non-core' flow (3–8; adjacent to the leaflets, hinge regions, and solid boundaries). Their corresponding shear stress loading waveforms (Figure 14b) were programmed into the HSD and their accentuated effect on platelet activation was measured as described in the methods. These trajectories represent the gamut of the shear stresses range for flow past MHVs. The corresponding platelet activation measurements (Figure 14c) show, as expected, significant differences between core and non-core trajectories ($p < 0.05$). The above case study demonstrates that geometry specific thrombogenic differences for a MHV can be identified and measured.
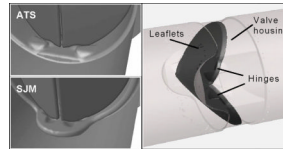
Figure 1.
Geometric details of the hinges regions of a 22 mm AP ATS open pivot valve and a 22 mm SJM Regent valve (both in closed position) – left. Geometric details of the bileaflet SJM MHV – right.
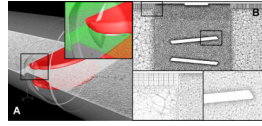
Figure 2.
(A) A horizontal cross-sectional plane showing the computational mesh near the open leaflets of the MHV. Inset shows the details of the computational grid near the hinges. (B) A vertical cross-sectional plane showing the computational mesh at the leaflets. The insets depict the boundary layers mesh near the wall (left) and the grid at the vicinity of the leaflet (right).
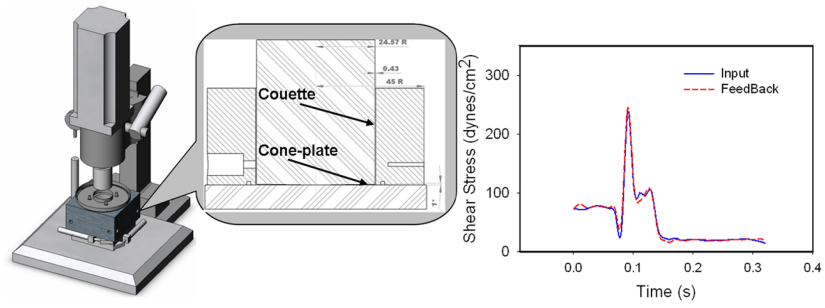
Figure 3.
Schematic of the Hemodynamic Shearing Device (HSD) and an example of accurate emulation of an highly dynamic platelet shear stress loading waveform that was extracted from a numerical simulation platelet trajectory in MHV.
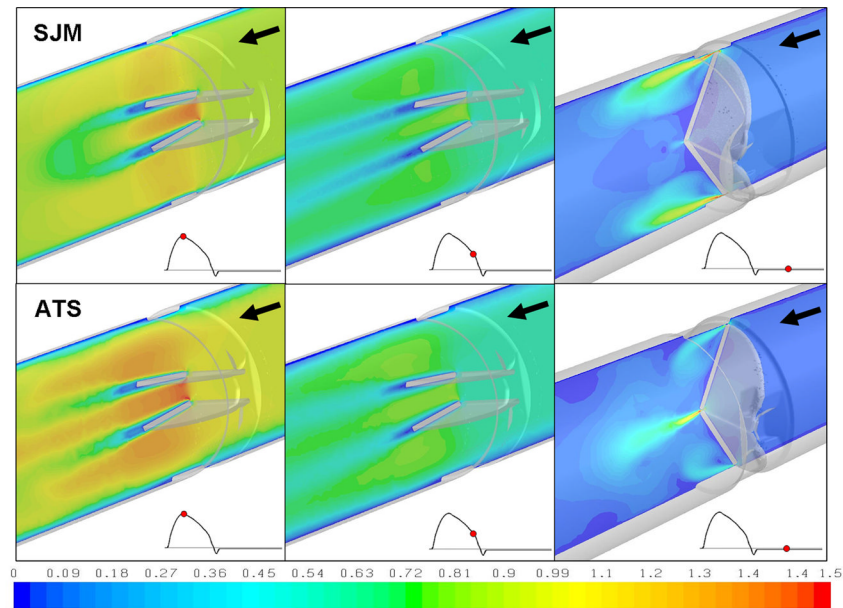
Figure 4.
Velocity flow field at the center plane for SJM and ATS MHV during the cardiac cycle. Three time instants are shown: peak systole, deceleration phase, and regurgitant flow through the closed valve during diastole. Arrows indicate the blood flow direction (valve geometry is reversed during the regurgitant flow phase to reveal the flow field behind the closed leaflets).
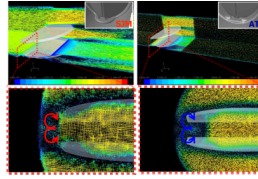
Figure 5.
A pair of counter-rotating vortices emanating from the jet flow that is generated in the hinges region of the SJM and ATS MHVs (transverse cross-section, details appear in the cross-sectional zoom-in–bottom). In an animation of the simulation (Animation 1) for the ATS valve the spinning of these counter rotating vortices is faster and entrained towards the core flow, while for the SJM larger counter rotating vortices are spinning slower and closer to the valve housing (the hinges are shown in the insets).
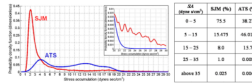
Figure 6.
Probability density function (PDF) of the stress accumulation (SA) distribution during the forward flow phase through the open valve for SJM, red line, and ATS, blue line. The distributions reveal the thrombogenic 'footprint' of each design. The inset indicates that at higher SA range (SA > 20 dyne×s/cm^2) the ATS appears to have an advantage over the SJM. Percentages of the number of platelets reaching a specific SA range appear in the table.
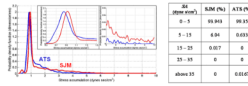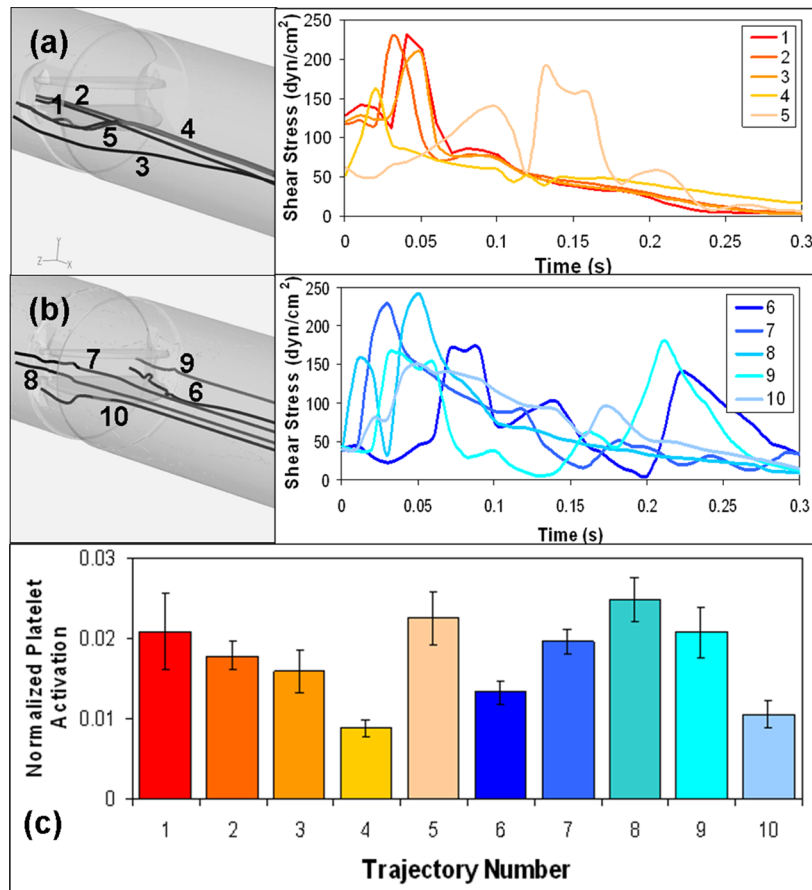
Figure 7.
Probability density function (PDF) of the stress accumulation (SA) distribution during regurgitation (SJM- red line, ATS- blue line). The details in the insets reveal the differences in the PDFs modes. At higher SA range the ATS appears to have a significant advantage over the SJM. Percentages of the number of platelets reaching a specific SA range appear in the table.

Figure 8.
Platelet experiments in the HSD emulating hinge region trajectories through the valves during forward flow: (a) SJM hinges trajectories (1–5) and the corresponding shear stress loading waveforms (b) ATS hinges trajectories (6–10) and the corresponding shear stress loading waveforms (c) Platelet activation corresponding to 600 repeats of each trajectory, measured with PAS.
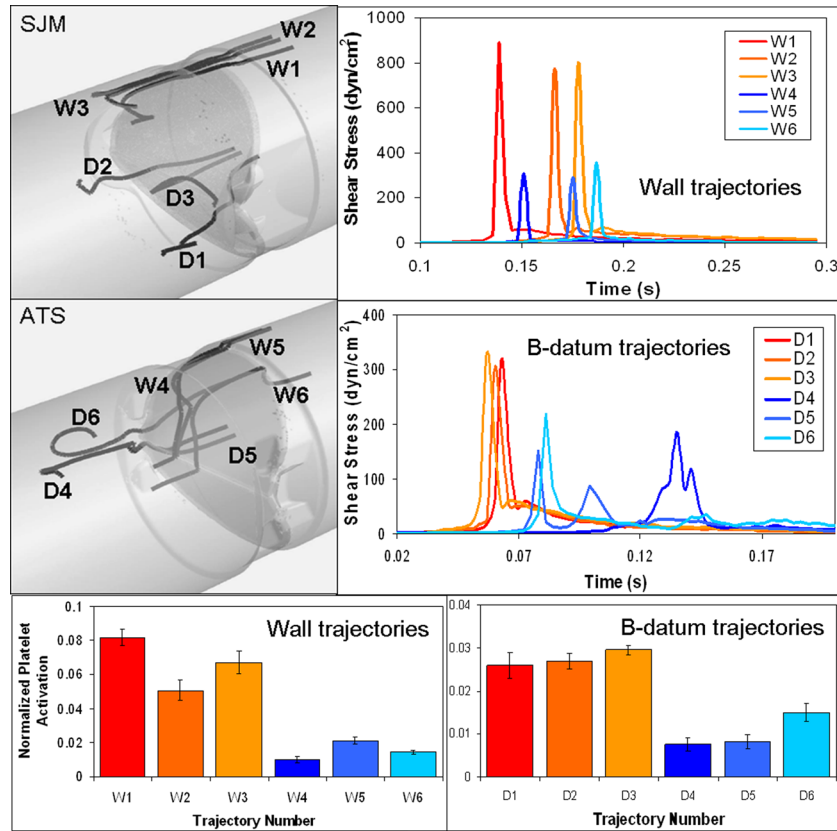
Figure 9.
Platelet experiments in the HSD emulating elevated shear stress trajectories through the valves during regurgitation; grouped into wall trajectories (W1–W3 SJM; W4–W6 ATS) and B-datum trajectories (D1–D3 SJM; D4–D6 ATS) (left) and the corresponding shear stress loading waveforms (right). The corresponding platelet activation in response to 600 repeats of each stress trajectory, measured with PAS appears at the bottom.
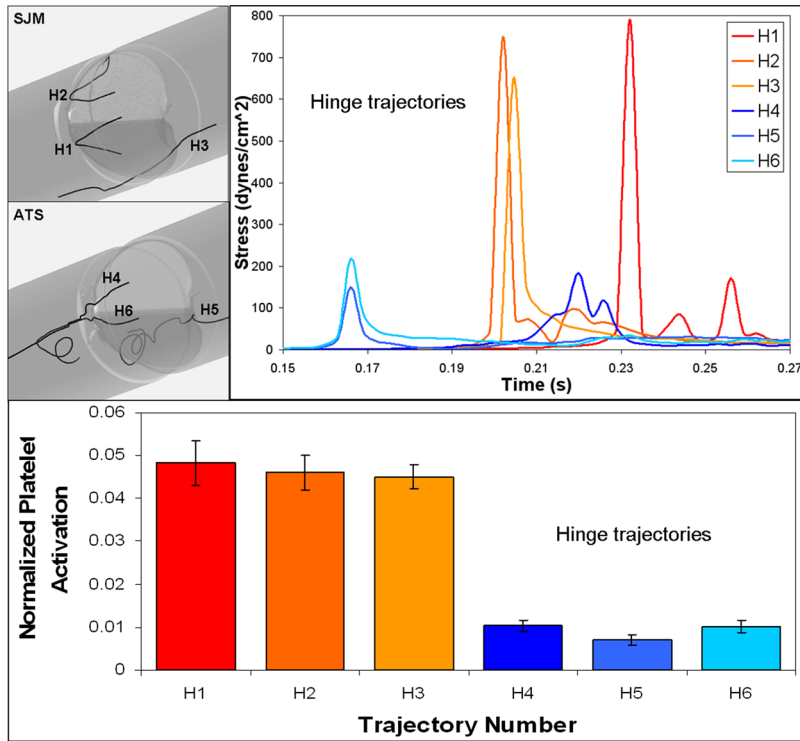
Figure 10.
Platelet experiments in the HSD emulating hinge region trajectories through the valves during regurgitation (H1–H3 SJM; H4–H6 ATS) and the corresponding shear stress loading waveforms (top). Platelet activation in response to 600 repeats of each stress trajectory, measured with PAS (bottom).
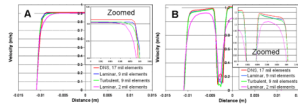
Figure 11.
Grid independence study: velocity profiles comparisons between the different numerical grid resolutions: 2, 9 and 17×10^6 finite volumes. The velocity profiles are extracted from cross-sections A and B in Figure 12.
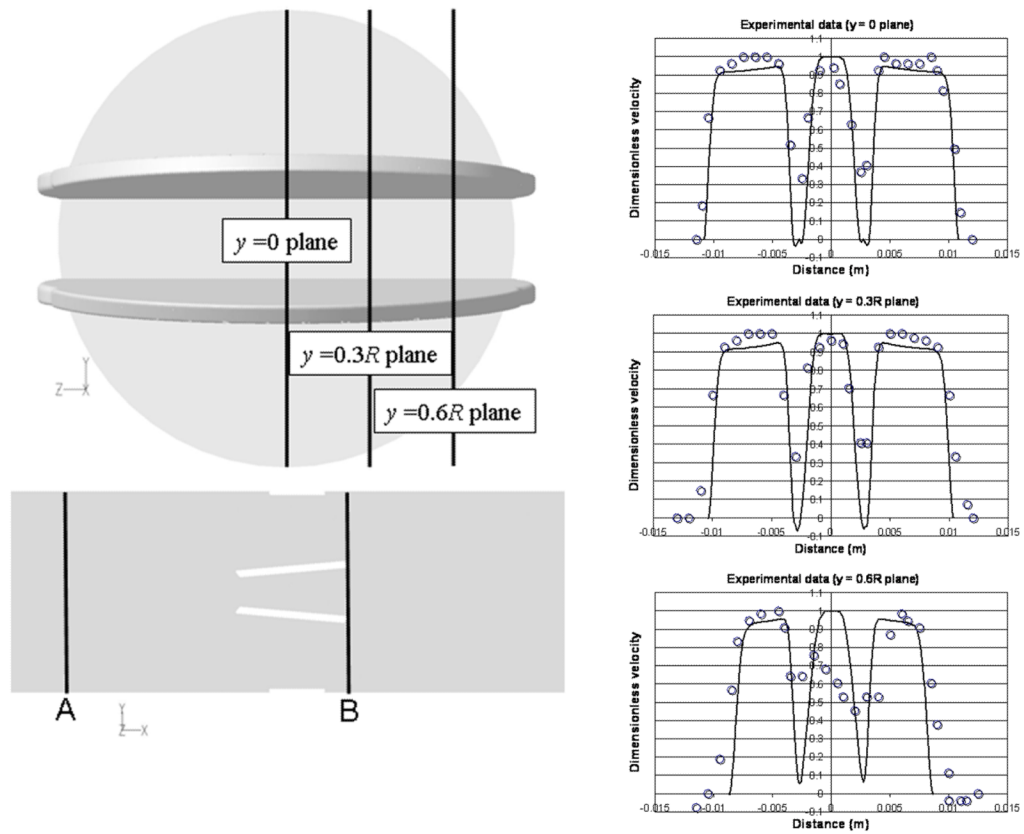
Figure 12.
Velocity profiles (Re ≈ 6,000) comparisons between the numerical simulations (solid lines), and experimental measurements from literature (open circles – Ge et al., 2005). The measurements are presented for cross-section B (left) at three vertical planes, y = 0, 0.3*R* and 0.6*R* planes (*R*- valve radius).
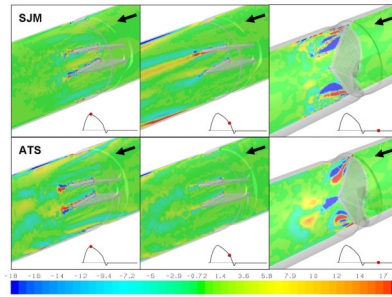
Figure 13.
Vorticity contours (ω_x) at the center plane for SJM and ATS MHV during three time instants in the cardiac cycle: peak systole, deceleration phase, and regurgitant flow through the closed valve during diastole. Arrows indicate the blood flow direction (valve geometry is reversed during the regurgitant flow phase to reveal the flow field behind the closed leaflets).
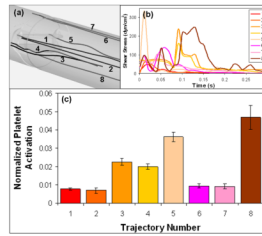
Figure 14.
Validation study of the HSD: platelet experiments in the HSD emulating core and non-core trajectories through the SJM-MHV during forward flow: (a) platelet trajectories extracted from the numerical simulations (b) the corresponding loading shear stress waveforms programmed into HSD (c) platelet activation in response to 600 repeats of each stress trajectory, measured with PAS.

Table 1

Valve diameters and gap clearance

	SJM (mm)	ATS (mm)
Valve diameter (Tissue Annulus Diameter)	22.0	22.0
Valve inner diameter	21.0	20.8
Gap clearance between hinge and leaflet	0.180	0.038
Gap clearance, closed position, leaflet and housing	0.173	0.127
B-datum gap, closed position	0.074	0.253

Table 2

Wilcox k-ω constants

$\alpha_\infty^* = 1$, $\alpha_\infty = 0.52$, $\alpha_0 = 1/9$, $\beta_\infty^* = 0.09$, $\beta_i = 0.072$

$R_\beta = 8$, $R_k = 6$, $R_\omega = 2.95$, $\zeta^* = 1.5$, $M_{t0} = 0.25$, $\sigma_k = \sigma_\omega = 2.0$